



HAL
open science

CFD Modelling of Breaking and Undular Tidal Bores with Physical Validation

X Leng, Pierre Lubin, Hubert Chanson

► **To cite this version:**

X Leng, Pierre Lubin, Hubert Chanson. CFD Modelling of Breaking and Undular Tidal Bores with Physical Validation. 37th IAHR World Congress, Aug 2017, Kuala Lumpur, Malaysia. pp.5072–5081. hal-02158917

HAL Id: hal-02158917

<https://hal.science/hal-02158917>

Submitted on 18 Jun 2019

HAL is a multi-disciplinary open access archive for the deposit and dissemination of scientific research documents, whether they are published or not. The documents may come from teaching and research institutions in France or abroad, or from public or private research centers.

L'archive ouverte pluridisciplinaire **HAL**, est destinée au dépôt et à la diffusion de documents scientifiques de niveau recherche, publiés ou non, émanant des établissements d'enseignement et de recherche français ou étrangers, des laboratoires publics ou privés.

CFD Modelling of breaking and undular tidal bores with physical validation

XINQIAN LENG⁽¹⁾, PIERRE LUBIN⁽²⁾ & HUBERT CHANSON⁽³⁾

⁽¹⁾ *The University of Queensland, School of Civil Engineering, Brisbane QLD 4072, Australia, xinqian.leng@uqconnect.edu.au*

⁽²⁾ *Université de Bordeaux, I2M, Laboratoire TREFLE, Pessac, France, lubin@enscbp.fr*

⁽³⁾ *The University of Queensland, School of Civil Engineering, Brisbane QLD 4072, Australia, h.chanson@uq.edu.au*

ABSTRACT

A tidal bore may form during spring tide conditions when the tidal range exceeds 4 to 6 m in a natural estuary with a funnel shaped river mouth and shallow initial water level. The propagation of tidal bores is a highly unsteady turbulent process associated with intensive sediment scouring and mixing. To date few physical and numerical studies documented the unsteady turbulent process of tidal bore propagation. Recent numerical CFD models lacked careful experimental validations. The present study aims to provide new results on CFD numerical modelling of tidal bore propagation with a wide range of Froude numbers (1.2 to 2.1) and systematic experimental validations. The model solved the incompressible Navier-Stokes equations in its two-phase flow forms using Large Eddy Simulation (LES). Both 2D and 3D simulations were conducted; the inlet turbulence of the 3D models was simulated by a Synthetic Eddy Method (SEM). The physical experiments were based upon an ensemble-average technique, with measurements of water depth and velocity repeated 25 times for each flow condition. The 2D CFD simulations showed good agreement in terms of free-surface elevations with experimental results, for the range of tested Froude numbers. Mesh grid refinement only improved the accuracy for some but not all flow conditions. The 2D velocity data showed qualitative and quantitative agreement, but only at a selective range of vertical elevation beneath the free-surface, where the inlet velocity were correctly reproduced. The 3D simulation highlighted a numerical boundary layer, the thickness of which agreed with the experimental results. The time-averaged velocity and velocity RMS of the numerical model data showed a closer agreement with the physical model outside the boundary layer. The development of the numerical boundary layer was clearly observed in the CFD model results.

Keywords: Tidal bores, CFD modelling, Large Eddy Simulation LES, physical model validation, turbulence

1 INTRODUCTION

The propagation of tidal bores is a highly unsteady turbulent process, associated with intensive sediment scouring and mixing. The occurrence of a tidal bore is marked by a steep rise in free-surface propagating upstream. A tidal bore could form during spring tide conditions when the tidal range exceeds 4 to 6 m in a natural system with a funnel shaped river mouth and shallow initial water level (Chanson, 2011) (Fig. 1). The strength of a tidal bore is characterised by its Froude number defined as:

$$Fr_1 = \frac{U + V_1}{\sqrt{g \times \frac{A_1}{B_1}}} \quad [1]$$

where U is the bore celerity positive upstream, V_1 is the streamwise velocity of the initially steady flow positive downstream, g is the gravitational acceleration: $g = 9.8 \text{ m/s}^2$, A_1 and B_1 are the cross-sectional area and width respectively for the initially steady flow. When the Froude number is less than unity, a bore cannot form. When the Froude number is between 1 and 1.2-1.3, the bore is undular (Treske, 1994; Koch & Chanson, 2008; Leng & Chanson, 2016a). When the Froude number exceeds 1.3-1.5, the bore is breaking, and its strength increases with increasing Froude number (Hornung et al., 1995; Koch & Chanson, 2009; Chanson, 2010; Leng & Chanson, 2016a).

To date limited physical studies studied the unsteady turbulent propagations of tidal bores (Hornung et al., 1995; Koch & Chanson, 2009; Chanson, 2010, 2011; Docherty & Chanson, 2012; Khezri & Chanson, 2012b; Leng & Chanson, 2015a,b,2016a,2017). Recent numerical studies were performed using Computational Fluid Dynamics (CFD) models (Furuyama & Chanson, 2010; Lubin et al., 2010a,b; Reichstetter, 2011; Simon et al., 2011; Chanson et al., 2012; Khezri, 2014; Simon, 2014), albeit over a limited range of Froude numbers and most lacked careful experimental validations. The present work presents new results on a numerical CFD model of the unsteady turbulent propagations of tidal bores in open channel flows, with a wide range of

Froude numbers (from 1.2 to 2.1). Both two-dimensional and three-dimensional CFD models were simulated. The modelling results were validated against physical experiments conducted systematically for the exact flow conditions used in the CFD models. The experiments were performed in a 19 m long 0.7 m wide rectangular prismatic channel. Ensemble-averaged flow measurements were performed, where experiments were repeated 25 times for each controlled flow conditions and the results were ensemble-averaged. The free-surface variations were measured by a series of acoustic displacement meters (ADMs) along the channel centerline, and the velocity characteristics were measured using a Nortek™ Vectrino+ acoustic Doppler velocimeter (ADV). All instruments were sampled at 200 Hz and synchronized within ± 0.01 s.



(a) Breaking tidal bore of Qiantang River (Laoyanchang, China), photograph taken on 23 September 2016.



(b) Undular tidal bore of Dordogne River (St. Pardon, France), photograph taken on 2 September 2015.

Figure 1. Photographs of tidal bores in rivers.

2 NUMERICAL METHOD AND CFD MODEL CONFIGURATION

2.1 Numerical method and implementation

The numerical modelling was conducted using the CFD code Thétis developed by the I2M laboratory, University of Bordeaux, France. The model solves the Navier-Stokes equations in its incompressible two-phase flow form between non-miscible fluids. In this case, the two fluids were air and water respectively. A phase function C , called the color function, is used to locate the different fluids with $C = 0$ in the air, $C = 1$ in water, with $C = 0.5$ the value assumed to characterise the interface location. The governing equations are presented below, which is the Large Eddy Simulation (LES) of an incompressible fluid flow classically derived by applying a convolution filter to the unsteady Navier-Stokes equations:

$$\nabla \cdot \bar{\mathbf{u}} = 0 \quad [2]$$

$$\rho \left(\frac{\partial \bar{\mathbf{u}}}{\partial t} + \bar{\mathbf{u}} \cdot \nabla \bar{\mathbf{u}} \right) = -\nabla p + \rho \bar{\mathbf{g}} + \nabla \cdot (\mu + \mu_t) [\nabla \bar{\mathbf{u}} + \nabla^T \bar{\mathbf{u}}] \quad [3]$$

and,

$$\frac{\partial C}{\partial t} + \bar{\mathbf{u}} \cdot \nabla C = 0 \quad [4]$$

where \vec{u} is the velocity, C is the phase function, t is the time, p is the pressure, \vec{g} is the gravity vector, ρ is the density, μ is the dynamic viscosity and μ_t is the turbulent viscosity. The turbulent viscosity μ_t is calculated with the Mixed Scale model (Sagaut, 2006), which was found to be accurate for coastal applications (Helluy et al., 2005; Lubin et al., 2006). The magnitude of the physical characteristics of the fluids was calculated based upon the phase function as:

$$\rho = C \times \rho_1 + (1 - C) \times \rho_0 \quad [5]$$

$$\mu = C \times \mu_1 + (1 - C) \times \mu_0 \quad [6]$$

The densities ρ_0 , ρ_1 and dynamic viscosities μ_0 , μ_1 are the respective properties of fluids 0 and 1: in this case, air and water respectively. The velocity and pressure coupling is solved with a pressure correction method (Goda, 1978).

The space derivatives of the inertial term are discretised by a hybrid upwind-centered scheme and the viscous terms is approximated by a second-order centered scheme (Lubin et al., 2006). The interface tracking is done using a Volume Of Fluid (VOF) method with a piecewise linear interface calculation (PLIC). This method has the advantage of building a sharp interface between air and water. The time discretization is implicit and the equations are discretised on a staggered grid thanks to a finite volume method. The MPI library HYPRE is used to solve the linear system of the prediction and correction steps (Falgout et al., 2006). The time steps are dynamically calculated to insure a CFL condition inferior to 0.2. The numerical model has been proved accurate through a variety of coastal applications and numerous test cases (Lubin, 2004; Lubin et al., 2006). Earlier CFD studying of tidal bores by Simon et al. (2011) and Khezri (2014) were also based upon this model.

2.2 Numerical model configuration

Both 2D and 3D CFD simulations were conducted in the present study. For 2D CFD simulations, breaking bores of $Fr_1 = 1.5$ and 2.1 , and undular bores of $Fr_1 = 1.2$ were modelled numerically. The numerical domain was 12 m in the longitudinal (stream-wise) direction and 1 m in the vertical direction (Fig. 2). A no-slip condition was imposed at the lower boundary ($z = 0$ m) and a Neumann condition was used at the upper boundary ($z = 1$ m). At the end of domain ($x = 12$ m), a wall boundary was imposed to act like a closed gate to reproduce the experimental generation process. The opening under the gate h_{out} could be set to introduce a Neumann condition between the bed ($z = 0$ m) and the bottom of the gate ($z = h_{out}$). The initial conditions of the 2D models consisted of a water trapezoid, with higher depth at the inlet (d_{in}) and lower depth at the outlet (d_{out}) to approximated the gradually-varied flow in the physical open channel. All initial and boundary parameters were taken from the experimental measurements.

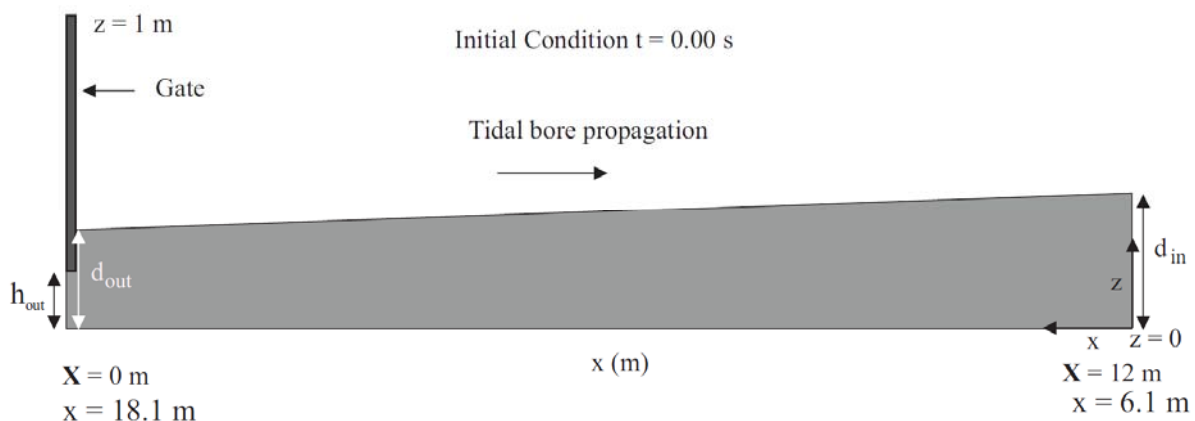


Figure 2. Definition sketch of numerical domain configurations; X is the distance from the left boundary (i.e. gate) of the numerical domain; x is the distance from the upstream end of the physical channel.

For 3D CFD simulations, the work is still in progress. Herein, only data of the initially steady flow before the bore arrival will be presented. The flow conditions simulated by the 3D CFD model corresponded to the initially steady flow before the breaking bore of $Fr_1 = 2.1$. The 3D model was based upon the 2D model configuration, extruded in the third direction being the transverse y dimension. The coordinate y was positive towards the left side wall and the 3D numerical domain was 0.7 m wide. In this case, no-slip conditions were applied to both lateral walls and bottom of the domain. The Synthetic Eddy Method (SEM) was used in the 3D model to inject turbulence at the inlet of the domain (Jarrin et al., 2006,2009). The input parameters for this

method, including mean velocity and velocity fluctuations, were all extracted from the experimental data of Leng & Chanson (2016a). The number of eddies was set at 2000 and the size of eddies was 0.010 m, which was an order of magnitude higher than the experimental data (Leng & Chanson, 2017). Jarrin et al. (2006,2009) found that the method gave better results with over-estimated eddy size. Table 1 documents detailed configurations of the 2D and 3D numerical models.

Table 2 summarises the experimental flow conditions corresponding to the three Froude number modelled by CFD ($Fr_1 = 1.2, 1.5, 2.1$). The reference depth d_1 and celerity U was taken at the velocity sampling location, which was located 9.6 m upstream of the gate for both physical and numerical channels.

Table 1. Initial configuration of the 2D and 3D numerical simulations.

Reference	Domain (m)	Mesh grid density	Fr_1	Q (m ³ /s)	S_o	d_{in} (m)	d_{out} (m)	h_{out} (m)	Bore type
2D_Fr1.2	12×1	1600×100	1.2	0.101	0	0.208	0.19	0.071	Undular
2D_FR1.5	12×1	2400×200	1.5	0.101	0	0.18	0.16	0	Breaking
2D_FR2.1	12×1	1600×140	2.1	0.101	0.0075	0.1	0.1	0	Breaking
3D_FR2.1	12×1×0.7	1600×250×200	2.1	0.101	0.0075	0.093	0.093	0	Breaking

Table 2. Flow conditions of the experimental data used to validate the numerical model.

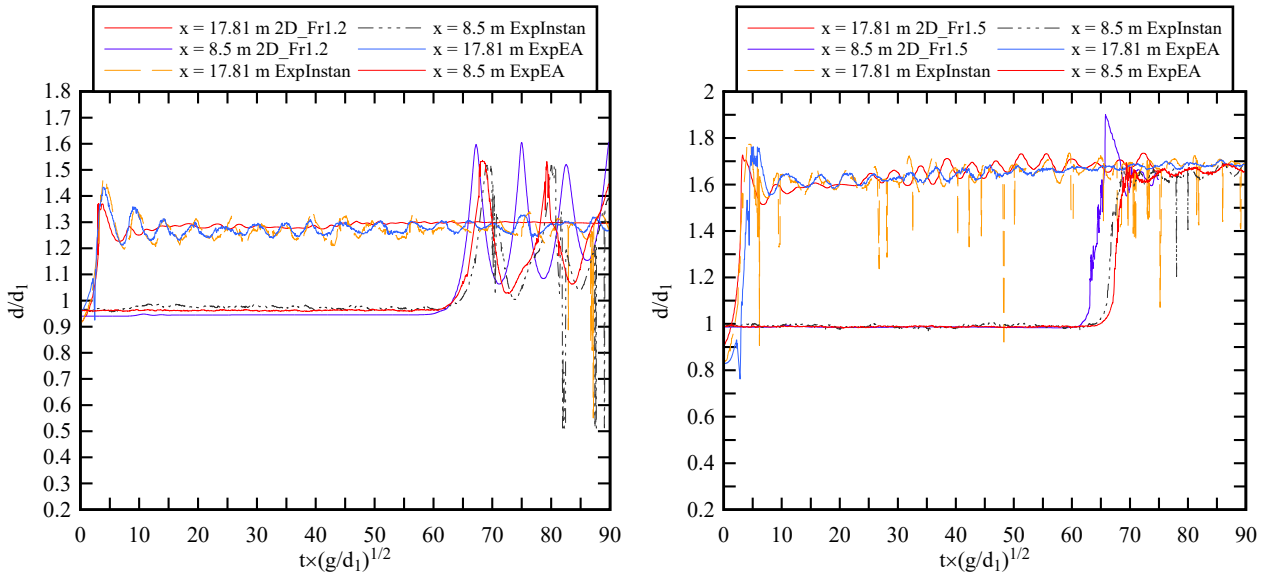
Reference	Fr_1	Q (m ³ /s)	S_o	d_1 (m)	U (m)	Bore type	Instrumentation
Leng & Chanson (2016a)	1.2	0.101	0	0.210	0.71	Undular	ADMs and ADV
	1.5	0.101	0	0.180	1.13	Breaking	ADMs and ADV
	2.1	0.101	0.0075	0.100	1.00	Breaking	ADMs and ADV

3 2D SIMULATION OF TIDAL BORE PROPAGATION

3.1 Free-surface comparisons

During the physical experiments, both instantaneous and ensemble-averaged measurements were performed to characterise the free-surface and velocity properties. Up to 10 acoustic displacement meters (ADMs) were installed at different longitudinal positions x (x = longitudinal distance from upstream end) on the channel centerline, all sampling at 200 Hz, to record the free-surface variations with time at different locations along the channel. During the numerical simulations, the free-surface variations with time were recorded at the same locations as those of the ADMs to validate the numerical results. Comparisons between numerically simulated free-surface evolution and experimental observations were conducted, and typical results are presented in Figure 3 for both undular and breaking bores. Note that the gate was located at $x = 18.1$ m.

Overall, the free-surface variations simulated by the 2D CFD model agreed well with the experimental data (instantaneous or ensemble-averaged) at all longitudinal locations, quantitatively and qualitatively, for all Froude numbers. Some deviations were observed in terms of the bore height and bore celerity. At generation (close to the gate), the numerical model tended to estimate relatively accurately the free-surface rise mechanism, with almost identical depth gradient with time. However the bore height was underestimated for both breaking and undular bores at generation. As the bore propagated upstream towards mid-channel, the numerical model overestimated the bore celerity and bore height, resulting in differences in terms of bore arrival time at $x = 8.5$ m (Fig. 3). For undular bores, the numerical model was associated with secondary wave periods which differed from the experimental data. The wave forms of the numerical model appeared to be more regular than the experimental data, due to the two-dimensional constraint and the absence of side wall effects.



(a) Undular bore ($Fr_1 = 1.2$)

(b) Breaking bore ($Fr_1 = 1.5$)

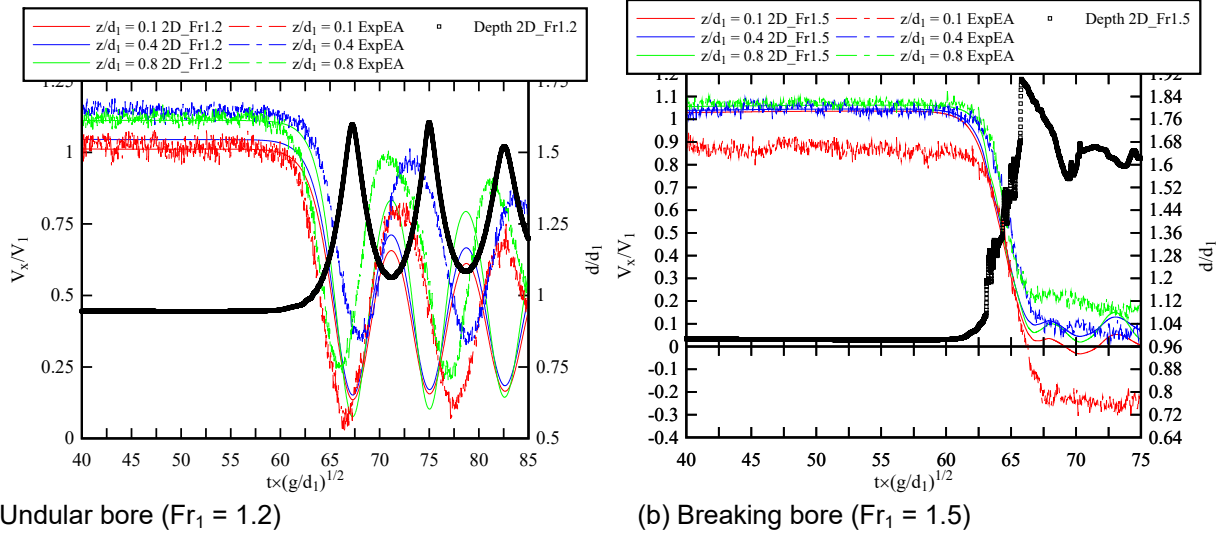
Figure 3. Dimensionless free-surface time evolution for undular and breaking bores of $Fr_1 = 1.2$ and 1.5 , respectively; Comparisons between numerical simulation (2D_Fr), instantaneous experimental data (ExpInstan) and ensemble-averaged experimental data (ExpEA).

3.2 Velocity comparisons

Ensemble-averaged velocity measurements were performed using a NortekTM Vectrino+ acoustic Doppler velocimeter (ADV) located on the channel centerline at mid-channel ($x = 8.5$ m). The ADV was equipped with a three-dimensional side looking head, able to record velocity in the longitudinal, transverse and vertical directions. The ADV was sampled at 200 Hz, synchronised with the ADMs, and measured velocity at a number of vertical elevations ($z/d_1 = 0.1, 0.4, 0.8$). During the numerical CFD modelling, velocity data at the same dimensionless vertical elevations was recorded at $x = 8.5$ m for validation purposes. Figure 4 presents typical comparisons between numerical and experimental results for bores with $Fr_1 = 1.2$ and 1.5 . The time frames of the numerical and experimental data was synchronized using the numerical time line.

Overall, the time-variations of the numerically-simulated velocity data agreed well with the experimental data at all vertical elevations and for all velocity components. The longitudinal velocity was associated with a sharp deceleration following the arrival of breaking bores. The vertical velocity showed a sharp acceleration then deceleration following the breaking bore arrival. One feature which was absent from the numerical data set was the presence of a boundary layer in the initially steady flow as shown in the experimental results. Although a no-slip condition was imposed at the bottom boundary of the model, resulting in slightly lower steady flow velocity for lower vertical elevations (Fig. 4), no obvious boundary layer such as highlighted in the experimental data was observed. This would be further addressed in the 3D simulation documented in Section 4.

Despite the absence of boundary layer, the present numerical data successfully reproduced the recirculation velocity in the longitudinal direction for the lowest vertical elevation during the propagation of breaking bores with complete gate closure (Fig. 4). Field and experimental studies have documented the presence of longitudinal recirculation at low vertical elevations (often $0 < z/d_1 < 0.3-0.5$) beneath the bore front for both breaking and undular bores (Wolanski et al., 2004, Chanson & Toi, 2015, Leng & Chanson, 2016a). This is characterised by a negative longitudinal velocity at the end of the deceleration following the bore passage, highlighted by the experimental data of breaking bores at $z/d_1 = 0.1$ in Figure 4b. The numerical data at the same dimensionless vertical elevation reproduced the recirculation velocity, however with a time delay (red solid curve in Fig. 4b).



(a) Undular bore ($Fr_1 = 1.2$) (b) Breaking bore ($Fr_1 = 1.5$)
Figure 4. Dimensionless time-variations of longitudinal velocity for undular and breaking bores of $Fr_1 = 1.2$ and 1.5 , respectively; Comparisons between numerical simulation (2D_Fr) and ensemble-averaged experimental data (ExpEA).

The undular bore was characterised by a gentle free-surface rise, followed by a series of well-formed secondary waves. Meanwhile, the longitudinal velocity decreased in a smooth manner with the rise of free-surface, and oscillated quasi-periodically with the free-surface by a phase difference of π . The vertical velocity increased with the free-surface rise, then oscillated quasi-periodically with the free-surface by a phase difference of $\pi/2$. The numerical results reproduced the periodic oscillations in the free-surface, longitudinal and vertical velocity variations, however with periods different from the experimental data. More specifically, the numerical data was associated with a shorter period. The minimum longitudinal velocity reached by the numerical model was higher than the experimental data, whereas the maximum longitudinal velocity of the secondary waves was lower than the experimental data (Fig. 4). The difference was believed to be due to the lack of the third dimension and of sidewall friction, and hence resulting in a more energetic behavior of the bore.

3.3 Discussion

The 2D numerical modelling results showed large vortical structures formed both underneath and behind the front of breaking bores (Fig. 5). Previous 2D CFD modelling by Khezri (2014) observed large vortical structures formed close to the bed, with a vertical dimension L_z up to 0.1 m ($L_z/d_1 \approx 0-0.5$) underneath breaking bores of Froude number 1.5. The present study highlighted two types of vortical structures, one near the fluctuating free-surface behind the roller, and one close to bed. The vortical structures near the upper free-surface were observed almost immediately downstream of the breaking roller, with length scales of $L_x \approx 0.1$ m ($L_x/d_1 \approx 0.56$), and were advected downstream as the bore front propagated upstream. This type of vortical structures were formed by the plunging mechanism of the steepened bore front into the flow and was typically associated with pockets of air.

The vortical structures next to the bed were observed to be flat and elongated, with much larger length scales in the longitudinal direction compared to the vertical direction. The height of these vortical structures was approximately $L_z \approx 0.02$ m ($L_z/d_1 \approx 0.11$). Experimental studies of turbulent scales by Leng and Chanson (2017) highlighted presence of anisotropic vortical structures underneath the bore front. The vertical length scale L_z was up to 0.02 m ($L_z/d_1 \approx 0-0.11$) for breaking bores with relatively large Froude numbers ($Fr_1 \geq 1.5$). The numerical results agreed with the experimental findings in terms of the vertical length scale of the vortical structures near the bed. The occurrence of vortical structures in the numerical model was found to be approximately 1 m downstream of the bore front, which was greatly delayed compared to experimental observations and past numerical results. The reason could be due to the 2D constraint, where bubble breakup mechanism was not allowed. Some numerical air bubbles were still observed more than 2 m ($\Delta x/d_1 \approx 0-11$) following the leading edge of the bore, while the entrained bubbles would have risen to the free-surface in a real physical flow (Wang et al., 2017).

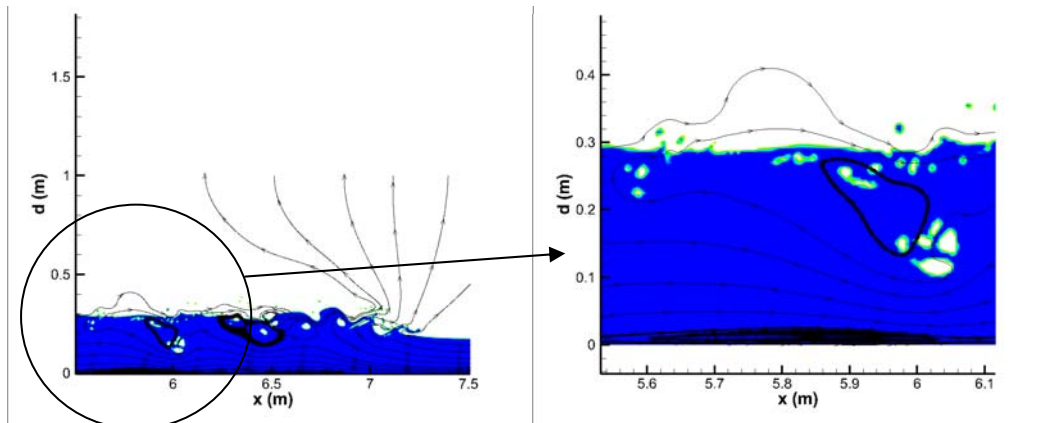


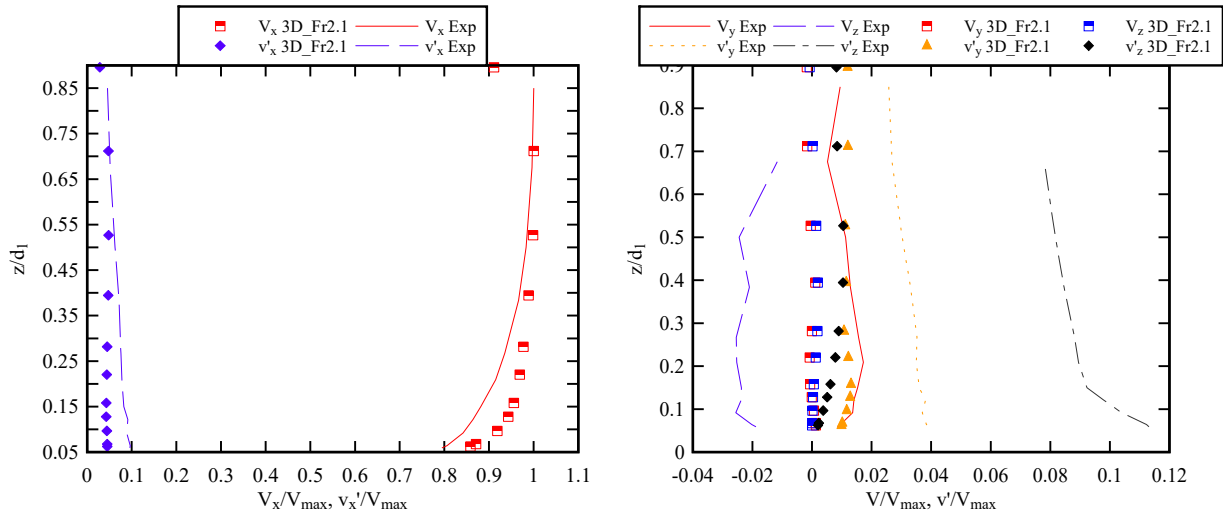
Figure 5. Vortical structures observed beneath the tidal bore.

4 3D STEADY FLOW SIMULATION

Figure 5 presents the vertical profile of the time-averaged velocity V and velocity fluctuations v' simulated by the 3D CFD model, compared to the experimental data. The time span of the numerical simulation was around 10 s, and the turbulence arrived at the velocity sampling location approximately after 1 s. The experimental data was time-averaged over 30 s. As highlighted in Figure 6a, the numerical profile of the longitudinal velocity clearly showed a bottom boundary layer. The vertical profile of the longitudinal velocity simulated by the numerical model agreed well in shape and values with the experimental data, especially at the outer edge and outside of the boundary layer, except for the highest vertical elevation. Inside the boundary layer, the numerical data agreed better with the experimental data close to bed, then deviated from the experimental curve, before they coincided again near the outer edge. The longitudinal velocity fluctuations, highlighted by its standard deviation, agreed quantitatively and qualitatively with the experimental data, with better fit near the outer edge and outside of the boundary layer.

The vertical profile of the transverse and vertical velocity components simulated by the numerical model showed very small, near-zero magnitudes. The values were orders of magnitudes smaller than the experimental data throughout the vertical range. The velocity fluctuations in the transverse and vertical directions were associated with values higher than the corresponding velocity component magnitudes, highlighted by the numerical data. Further, the numerical data showed increase in velocity fluctuations with increasing vertical elevations, which agreed in terms of trend to the experimental data. Nevertheless, the experimental fluctuations were orders of magnitudes higher than the numerical ones, especially in the vertical direction. This could be attributed to the arrangement of the ADV head, which was known to over-estimate the vertical velocity fluctuations because of beam reflections and echo effects on the bed.

From the time series, turbulence was observed to arrive at the velocity sampling point after approximately 1 s and was fully developed after 5 s. The evolution of the numerical boundary layer was thus studied by time-averaging the longitudinal velocity at different vertical elevations over different time spans, from the entire time span of 10.609 s down to every 2 s. The results are presented in Figure 7, with comparison to experimental data. Overall, all numerical profiles were associated with the presence of boundary layers. The point at the highest vertical elevations ($z/d_1 = 0.90$) was associated with outlying values at all time. This was previously observed by Simon (2014) using the same numerical tool. For all time spans, the numerical data showed better agreement near the bottom and close to the outer edge of the boundary layer. Throughout the vertical range, the accuracy of the data seemed to be unaffected by the time span over which the numerical data was averaged, as long as the turbulence has reached the velocity sampling location. The findings seemed to suggest that, once the flow became turbulent and the boundary layer started to develop in the numerical model, the steady flow data would not evolve with longer time of simulation. The finding indicated good quality of numerically simulated turbulence, and highlighted the importance of using the actual experimental data for the numerical inlet boundary.



(a) Longitudinal velocity

(b) Transverse and vertical velocity

Figure 6. Vertical time-averaged velocity profile of the steady flow longitudinal (a), transverse and vertical (b) velocity components; Comparison between numerical (3D_Fr2.1) and experimental results (Exp).

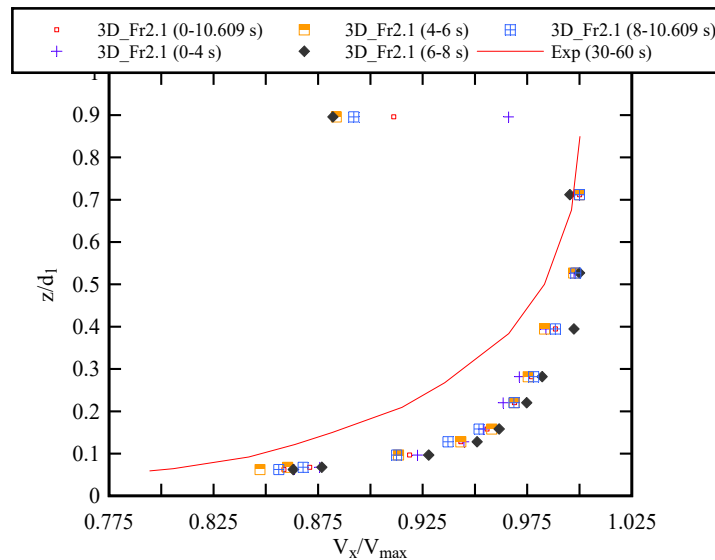


Figure 7. Vertical profile of time-averaged longitudinal velocity, simulated by the numerical model and averaged over different time span (3D_Fr2.1).

5 CONCLUSION

The propagation of tidal bores in open channels was investigated numerically using 2D and 3D CFD model with Large Eddy Simulations. The numerical modelling investigated tidal bores with Froude numbers ranging from 1.2 to 2.1. The results of the numerical studies were compared and validated against experimental data collected under the same flow conditions. Overall, the 2D numerical results gave good approximation of the free-surface elevation associated with the bore propagation for the range of Froude numbers. The modelled velocity data agreed well with the experimental data outside the boundary layer, and highlighted some longitudinal recirculation underneath breaking bores, although with a delayed occurrence. The numerical model tended to over-estimate the bore celerity and under-estimate the bore height for both breaking and undular bores. Streamline tracing of the numerical results highlighted elongated thin vortical structures behind the bore front and close to bed, with vertical length scale comparable to experimental findings. The 3D steady flow results highlighted a developing boundary layer in the initially steady flow before the bore generation. The thickness of the boundary layer was comparable to experimental results, and the numerical and experimental velocity profiles agreed closely next to the bottom and near the outer edge of the boundary layer. The development of the numerical boundary layer over time was examined. Results suggested that after the turbulence has reached the velocity sampling location, the numerical boundary layer changed very little with longer simulation time.

ACKNOWLEDGMENTS

The authors acknowledge Dr. Stéphane Glockner (Université de Bordeaux, I2M, Laboratoire TREFLE, Pessac, France) for his expert assistance. The authors also wish to thank the Aquitaine Regional Council for financial support towards a 432-processor cluster investment, located in the I2M laboratory. This work was granted access to the HPC resources of CINES, under allocation 2016-x2012026104 made by GENCI (Grand Equipement National de Calcul Intensif). Computer time for this study was also provided by the computing facilities at MCIA (Mésocentre de Calcul Intensif Aquitain) of the Université de Bordeaux and of the Université de Pau et des Pays de l'Adour. The financial support of the Graduate Student International Travel Award provided by UQ Graduate School is acknowledged.

REFERENCES

- Chanson, H. (2011). *Tidal Bores, Aegir, Eagre, Mascaret, Pororoca: Theory and Observations*. World Scientific, Singapore, 220 pages (ISBN 9789814335416).
- Chanson, H., & Toi, Y.H. (2015). Physical modelling of breaking tidal bores: comparison with prototype data. *Journal of Hydraulic Research*, IAHR, 53 (2), 264-273.
- Chanson, H., Lubin, P. and Glockner, S. (2012). Unsteady turbulence in a shock: physical and numerical modelling in tidal bores and hydraulic jumps. *Turbulence: theory, types, and simulation*, Nova Science Publishers, Hauppauge, N.Y: R.J. Marcuso, 3, 113–148.
- Falgout, R., Jones, J. and Yang, U. (2006). The design and implementation of hypre, a library of parallel high performance preconditioners. *Numerical solution of partial differential equations on parallel computers*, Lecture notes in computational science and engineering. Springer Berlin Heidelberg, 51.
- Furuyama, S., and Chanson, H. (2010). A Numerical Solution of a Tidal Bore Flow. *Coastal Engineering Journal*, 52 (3), 215-234 (DOI: 10.1142/S057856341000218X).
- Goda, K. (1979). A multistep technique with implicit difference schemes for calculating two-or three-dimensional cavity flows. *Journal of Computational Physics*, 30 (1), 76-95.
- Helluy, P. et al. (2005). Numerical simulations of wave breaking. *ESAIM: Mathematical Modelling and Numerical Analysis*, 39 (03), 591-607.
- Hornung, H.G., Willert, C., and Turner, S. (1995). The Flow Field Downstream of a Hydraulic Jump. *Journal of Fluid Mechanics*, 287, 299-316.
- Jarrin, N., S. Benhamadouche, D. Laurence, and R. Prosser (2006). A synthetic-eddy method for generating inflow conditions for large-eddy simulations. *International Journal of Heat and Fluid Flow*, 27 (4), 585–593.
- Jarrin, N., R. Prosser, J.-C. Uribe, S. Benhamadouche, and D. Laurence (2009). Reconstruction of turbulent fluctuations for hybrid RANS/LES simulations using a Synthetic-Eddy Method. *The Seventh International Symposium on Engineering Turbulence Modelling and Measurements, ETMM7*, 30 (3), 435–442.
- Khezri, N. (2014). Modelling Turbulent Mixing and Sediment Process Beneath Tidal Bores: Physical and Numerical Investigations. *Ph.D. thesis*, School of Civil Engineering, The University of Queensland, Brisbane, Australia, 267 pages.
- Koch, C., and Chanson, H. (2008). Turbulent Mixing beneath an Undular Bore Front. *Journal of Coastal Research*, 24 (4), 999-1007 (DOI: 10.2112/06-0688.1).
- Koch, C., and Chanson, H. (2009). Turbulence Measurements in Positive Surges and Bores. *Journal of Hydraulic Research*, IAHR, 47 (1), 29-40 (DOI: 10.3826/jhr.2009.2954).
- Leng, X., and Chanson, H. (2015a). Turbulent Advances of a Breaking Bore: Preliminary Physical Experiments. *Experimental Thermal and Fluid Science*, 62, 70-77 (DOI: 10.1016/j.expthermflusci.2014.12.002).
- Leng, X., and Chanson, H. (2015b). Breaking Bore: Physical Observations of Roller Characteristics. *Mechanics Research Communications*, 65, 24-29 (DOI: 10.1016/j.mechrescom.2015.02.008) (ISSN 0093-6413).
- Leng, X., and Chanson, H. (2015c). Unsteady Turbulence during the Upstream Propagation of Undular and Breaking Tidal Bores: an Experimental Investigation. *Hydraulic Model Report No. CH98/15*, School of Civil Engineering, The University of Queensland, Brisbane, Australia, 235 pages & 4 video movies (ISBN 978 1 74272 135 4).
- Leng, X., and Chanson, H. (2016a). Coupling between Free-surface Fluctuations, Velocity Fluctuations and Turbulent Reynolds Stresses during the Upstream Propagation of Positive Surges, Bores and Compression Waves. *Environmental Fluid Mechanics*, 16 (4), pp. 695-719 & digital appendix (DOI: 10.1007/s10652-015-9438-8).
- Leng, X., and Chanson, H. (2016b). Unsteady Turbulent Velocity Profiling in Open Channel Flows and Tidal Bores using a Vectrino Profiler. *Hydraulic Model Report No. CH101/15*, School of Civil Engineering, The University of Queensland, Brisbane, Australia, 118 pages (ISBN 978-1-74272-145-3).
- Leng, X., and Chanson, H. (2017). Integral Turbulent Scales in Unsteady Rapidly Varied Open Channel Flows. *Experimental Thermal and Fluid Science*, 81, 382-395 (DOI: 10.1016/j.expthermflusci.2016.09.017).
- Lubin, P., (2004). Large Eddy Simulation of Plunging Breaking Waves. *Ph.D. Thesis*, Université Bordeaux I, France (in English).

- Lubin, P., H. Chanson, and S. Glockner (2010a). Large eddy simulation of turbulence generated by a weak breaking tidal bore. *Environmental Fluid Mechanics*, 10 (5), 587-602.
- Lubin, P., S. Glockner, and H. Chanson (2010b). Numerical simulation of a weak breaking tidal bore. *Mechanics Research Communications*, 37 (1), 119-121.
- Lubin, P., S. Vincent, S. Abadie, and J.-P. Caltagirone (2006). Three-dimensional large eddy simulation of air entrainment under plunging breaking waves. *Coastal Engineering*, 53 (8), 631-655.
- Reichstetter, M. (2011). Hydraulic Modelling of Unsteady Open Channel Flow: Physical and Analytical Validation of Numerical Models of Positive and Negative Surges. *MPhil Thesis*. Brisbane, Australia: School of Civil Engineering, The University of Queensland.
- Sagaut, P. (2006). *Large eddy simulation for incompressible flows: an introduction*. 3rd. Berlin, Heidelberg, New York: Springer-Verlag Berlin and Heidelberg.
- Simon, B. (2014). Effects of Tidal Bores on Turbulent Mixing: a Numerical and Physical Study in Positive Surges. *Ph.D. thesis*, School of Civil Engineering, The University of Queensland, Brisbane, Australia, 259 pages & 7 movies (DOI: 10.14264/uql.2014.19).
- Simon, B., P. Lubin, S. Glockner, and H. Chanson (2011). Three-dimensional numerical simulation of the hydrodynamics generated by a weak breaking tidal bore. In: *34th IAHR World Congress, 33rd Hydrology and Water Resources Symposium and 10th Conference on Hydraulics in Water Engineering*. Brisbane, Australia: Eric Valentine, Colin Apelt, James Ball, Hubert Chanson, Ron Cox, Robert Ettema, George Kuczera, Martin Lambert, Bruce Melville and Jane Sargison, 133-1140.
- Treske, A. (1994). Undular Bores (Favre-Waves) in Open Channels - Experimental Studies. *Jl of Hyd. Res., IAHR*, 32 (3), 355-370. Discussion: 33, (3), 274-278.
- Wang, H., Leng, X., and Chanson, H. (2017). Bores and Hydraulic Jumps. *Environmental and Geophysical Applications. Engineering and Computational Mechanics*, Proceedings of the Institution of Civil Engineers, UK, 170, paper 1600025, 18 pages (DOI: 10.1680/jenm.16.00025).
- Wolanski, E., Williams, D., Spagnol, S., and Chanson, H. (2004). Undular Tidal Bore Dynamics in the Daly Estuary, Northern Australia. *Estuarine, Coastal and Shelf Science*, 60 (4), 629-636 (DOI: 10.1016/j.ecss.2004.03.001).